Japan J. Indust. Appl. Math., 24 (2007), 67–77 Area ⟨1⟩

Most Stable Patterns among Three-Dimensional Turing Patterns

Hiroto Shoji*,† and Kohtaro Yamada†

* *Meiji Institute for Mathematical Sciences, Meiji University*
Higashimita, Tamaku, Kawasaki 214–8571, Japan
E-mail: hshoji@math.meiji.ac.jp
† *Yukawa Institute for Theoretical Physics, Kyoto University*
Kyoto 606–8502, Japan

Received June 9, 2006
Revised October 13, 2006

It is known that Turing systems in two dimensions produce spotted, striped, and labyrinthine patterns. In three dimensions, a greater variety of patterns is possible. By numerical simulation of the FitzHugh–Nagumo type of reaction-diffusion system, we have obtained not only lamellar, hexagonal and spherical structures (BCC and FCC) but also gyroid, Fddd, and perforated lamellar structures. The domains of these three structures constitute interconnected regular networks, a characteristic occurring in three dimensions. Moreover, we derive the Lyapunov functional by reducing the system, and we evaluate this functional by introducing the asymptotic solutions of each structure by the mode-expansion method and direct simulation of the time evolution equation.

Key words: Turing system, three-dimensional patterns, stability analysis, FitzHugh–Nagumo, interface

1. Introduction

Nature presents a fascinating diversity of patterns in plants, animals, and other natural formations in response to complex physico-chemical processes [1, 2]. Among such processes, Turing systems have received special attention since Turing showed that a coupled reaction-diffusion equation with two components admits spatially periodic solutions if certain conditions are satisfied [3]. This mechanism is now called "diffusion-driven instability" or "Turing instability" [2]. For the past five decades, Turing patterns have been studied numerically and analytically as examples of dissipative structures far from equilibrium [4]. It is well known that most of pattern formations not only in various biological phenomena [2] but also in chemical and physical systems [4] have been related to the Turing mechanism.

The first experimental evidence of Turing structure was reported in 1990 by Castets et al. [6], who observed a sustained standing non-equilibrium chemical pattern in an open chemical reactor with a chloride-iodide-malonic acid (CIMA) reaction. There has been increasing interest in the development of simple and plausible mathematical models that could describe these pattern formations [4, 5, 7].

The forms and variations of patterns generated by Turing systems have been studied analytically and numerically by investigating the conditions for instabilities. On the other hand, chemical experiments have confirmed both theoretical and numerical results and provided insight into the chemical dynamics of dissipative structures [5].

Although a lot of investigations thus far have been restricted to the one or two dimensions, there are few studies for Turing patterns in three dimensions. De Wit et al. [8,9] and Leppanen et al. [10] numerically found spherical domains in a body-centered cubic (BCC) lattice, hexagonally packed cylinders, and both lamellar and distorted lamellar structures. However, these structures in three dimensions are essentially related to structures in two dimensions.

In the present paper, we shall discuss three-dimensional Turing patterns in the FitzHugh–Nagumo type of reaction-diffusion model following our previous studies [11, 12]. Apart from lamellar and hexagonal structures that are simple generalizations of two-dimensional patterns, we have obtained gyroid, Fddd, BCC, and perforated lamellar structures. In this line of research, we explore the three-dimensional Turing patterns by a large number of computer simulations on the cubic domain $\Omega = [0, L]^3$ using not only various control parameters but also mesh size since the three-dimensional Turing patterns obtained depend strongly on the domain size L.

Because three or four different patterns are obtained at the same control parameter (see Fig. 1), the stability analysis of obtained patterns is one of the most fundamental problems. In this line of research we therefore address this problem also. Here we derive a Lyapunov functional considering the reduction of the systems, and we evaluate the functional by introducing the approximate solutions of domains by two methods (the mode-expansion method and direct simulation in the time evolution equation).

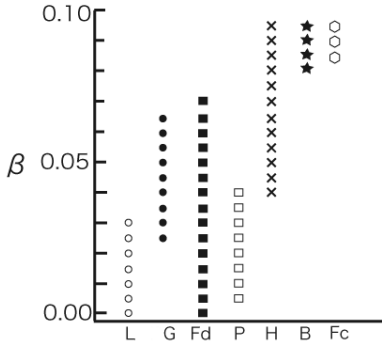

Fig. 1. Six stationary solutions. The meanings of L, G, Fd, P, H, B, and Fc are given in the text.

2. The model

Turing [3] showed that two diffusive chemicals reacting with each other locally could generate spatially heterogeneous patterns in a uniform field. The resulting system is written as

$$\begin{cases} \dfrac{\partial u}{\partial t} = D_u \nabla^2 u + f(u, v), \\ \dfrac{\partial v}{\partial t} = D_v \nabla^2 v + g(u, v), \end{cases} \tag{1}$$

where u and v are the concentrations of two substances that differ in diffusivity. Here we assume that v diffuses faster than u, and hence D_v is larger than D_u.

Turing [3] said that if, in the absence of diffusion (effectively $D_u = D_v = 0$), $u(t)$ and $v(t)$ of the corresponding ODEs tend to a linear stable uniform steady state, then under certain conditions spatially inhomogeneous patterns can evolve by diffusion-driven instability if $D_u \neq D_v$. This novel concept is called "diffusion-driven instability" or "Turing instability" [2].

We focus on the following the FitzHugh–Nagumo type of reaction-diffusion system [13, 14] with

$$\begin{aligned} f(u,v) &= u - u^3 - v, \\ g(u,v) &= \gamma(u - \alpha v - \beta), \end{aligned} \tag{2}$$

where the constants $\alpha, \beta, \gamma, D_u$ and D_v are all positive. This set of equations has been studied as a model of impulse propagation along nerve axons ($D_v = 0.0$) [15] as well as a model of the Belousov–Zhabotinsky chemical reaction $\alpha, \beta, \gamma, D_u$ and D_v ($D_u \geq D_v$) [16]. Therefore, it is well known that the reaction diffusion system (1) and (2) shows a variety of spatio-temporal patterns. Of course, the oscillatory phenomena and traveling wave occur in certain parameter regions. Here the parameters are restricted to fulfill the following conditions where Turing instability occurs.

One equilibrium solution (u_0, v_0) is given by $u_0 - u_0^3 - v_0 = 0$ and $u_0 - \alpha v_0 - \beta = 0$. The linear stability analysis of the uniform solution is carried out. Put $(u - u_0, v - v_0) \sim \exp(ikx + \lambda t)$. The solution becomes unstable if the following eigenvalue λ is positive,

$$\lambda^2 + \{(D_u + D_v)k^2 - (3u_0^2 + \alpha\gamma - 1)\}\lambda + (D_u k^2 + 3u_0^2 - 1)(D_v k^2 + \alpha\gamma) + \gamma = 0. \tag{3}$$

Solving this, we obtain the critical wave number

$$k_c^2 = \frac{1 - 3u_0^2}{2D_u} - \frac{\alpha\gamma}{2D_v}, \tag{4}$$

and the bifurcation threshold is given by

$$\frac{\{D_v(1 - 3u_0^2) - \alpha\gamma D_u\}^2}{4D_u D_v} + \alpha\gamma(1 - 3u_0^2) - \gamma > 0.$$

In a three-dimensional system, the wave number is of the form

$$\left|\vec{k}\right| = \frac{2\pi}{L}\sqrt{n_x^2 + n_y^2 + n_z^2},$$

where L is the domain size and n_x, n_y, n_z are the wave number indices.

There are several other choices of reaction terms f and g, such as the Brusselator [17] and the Gray–Scott models [18], which behave in ways similar

to the model proposed above. De Wit et al. [8, 9] and Leppanen et al. [10] studied three-dimensional Turing patterns using the Brusselator [17] and the Gray–Scott [18] types of reaction-diffusion systems, respectively.

3. Three-dimensional Turing patterns

We calculated the model given by equations (1) with (2) in three dimensions numerically. The space is divided into N^3 mesh points ($N = 32$), and periodic boundary conditions are imposed. To solve the equation, we used the simple Euler explicit method. To remove the anisotropy in discretizing the Laplacian, we employed a 27-point difference scheme [19].

In most simulations, we chose these parameters: $D_u = 5.0 \times 10^{-5}$, $D_v = 5.0 \times 10^{-3}$, $\gamma = 26.0$, and $\alpha = 0.50$. The parameter β is set as the control parameter. We also examined different parameter sets: $D_u = 5.0 \times 10^{-5}$, $D_v = 5.0 \times 10^{-4}$, $\gamma = 4.0$, and $\alpha = 0.50$, but the obtained results remained qualitatively the same. We also checked the dependency of the results on mesh size in the dividing space. We tested in the domains of $N = 50$ and $N = 64$, and the results were identical.

Although the domain size is not related to the Turing patterns obtained in two dimensions, the domain size is the critical point to determine Turing patterns in three dimensions. In our previous paper [11], we selected $L = 1.7 \times 10^{-1}$ (the linear dimension of the system is equal to $\delta x = 5.3 \times 10^{-3}$) as the domain size L.

Here, to explore the variety of obtained patterns, we perform computer simulations using not only various control parameters but also various domain size L. We change the domain size by 2.0×10^{-5} from $L = 1.0 \times 10^{-1}$ to $L = 2.5 \times 10^{-1}$.

We start with the unstable uniform solution (u_0, v_0) on which a small random perturbation is superimposed). To remove trapping at the metastable state, we introduce a Gaussian noise source $\xi = \xi(\vec{x}, t)$ to (1) such that

$$\begin{cases} \dfrac{\partial u}{\partial t} = D_u \nabla^2 u + f(u, v) + \xi_u, \\ \dfrac{\partial v}{\partial t} = D_v \nabla^2 v + g(u, v) + \xi_v, \end{cases} \tag{5}$$

where the first and second moments of ξ are defined as

$$\langle \xi(\vec{x}, t) \rangle = 0,$$
$$\langle \xi(\vec{x}, t) \xi(\vec{x}\,', t') \rangle = A^2 \xi(\vec{x} - \vec{x}\,') \xi(t - t').$$

The angular brackets denote an average and A is the intensity of the noise. Noise is added at every time step to each lattice site of the systems.

The asymptotic stationary solutions obtained are summarized in Fig. 1. This diagram was obtained by changing the five sets of random initial conditions for a given value of β and for a given mesh size. Note that three or four different structures coexist. The abbreviations L, H, and B refer to lamellar, hexagonal, and BCC structures, respectively. The remaining four structures, G, Fd, P, and Fc, are analyzed below.

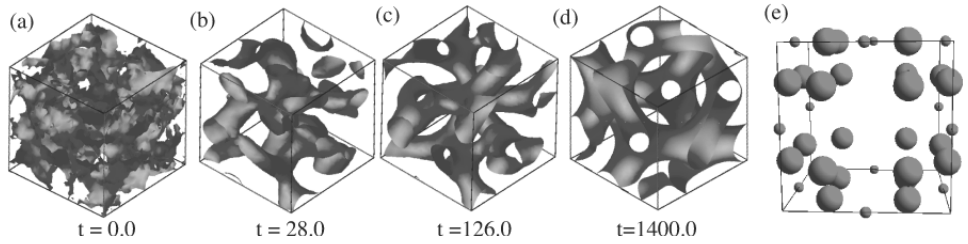

Fig. 2. (a)–(d) The structural evolution of domain for $\beta = 0.04$ and $L = 1.709 \times 10^{-1}$ ($\delta x = 5.34 \times 10^{-3}$), (e) the Bragg position of the structure. For the clarity, the domains in (a) represent the isosurface of $u = 0.08$, whereas those in the (b)–(d) isosurface of $u = 0.05$. (e) The radius of the spheres is proportional to the relative peak intensity. In this figure, as well as in Figs. 3–6 (b), the Bragg point at the origin is omitted.

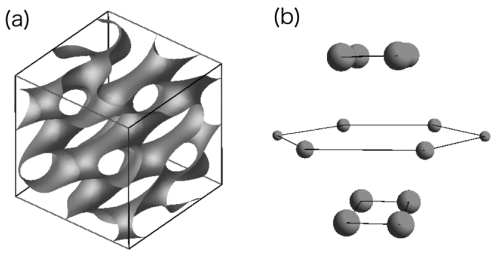

Fig. 3. (a) Fddd structure for $\beta = 0.04$ and $L = 1.626 \times 10^{-1}$ ($\delta x = 5.08 \times 10^{-3}$) represented by the isosurface of $u = 0.05$ and (b) are the same as those in Fig. 2 (e). The Bragg points on the same plane are connected by a line. Note that the quasi-proper hexagon and the two rectangles are parallel to each other.

To clarify the structures in Figs. 2–6, we carried out Fourier transformation of the asymptotic values of u and v. We evaluated the scattering intensity that has the following main peaks (in units of $2\pi/N$ apart from the origin $\mathrm{O} = (0, 0, 0)$).

Fig. 2 displays the formation of G and the peaks. Fig. 2 (a)–(d) show the isosurfaces of u. The distribution of v follows the one of u. Fig. 2 (e) shows the peaks of distribution of Fig. 2 (d). It is well known that a gyroid structure can be approximated by the following level set equation:

$$\begin{aligned} 0 = {} & 8(1-\eta)[\sin 2x \sin z \cos y + \sin 2y \sin x \cos z + \sin 2z \sin y \cos z] \\ & - 4\eta[\cos 2x \cos 2y + \cos 2y \cos 2z + \cos 2z \cos 2x] - \zeta, \end{aligned} \tag{6}$$

where η and ζ are the parameters [20]. The peak positions evaluated numerically are identical to the reciprocal lattice vector obtained from equation (6), by which we identify G with a gyroid structure.

The asymptotic domain structure of Fd and the peak positions are shown in Fig. 3. We omitted the peaks with smaller intensities than ten thousands part of the largest intensities of peaks. In Yamada et al. [21], the structures with peaks in

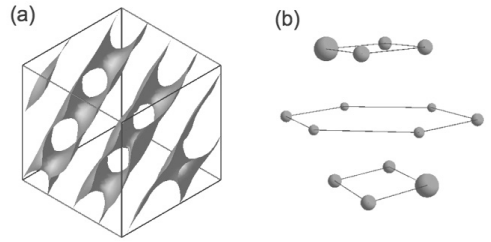

Fig. 4. (a) Perforated lamellar structure for $\beta = 0.04$ and $L = 1.626 \times 10^{-1}$ ($\delta x = 6.32 \times 10^{-3}$) represented by the isosurface of $u = 0.05$ and (b) the Bragg position with intensities. The details of (b) are the same as those in Fig. 2 (e).

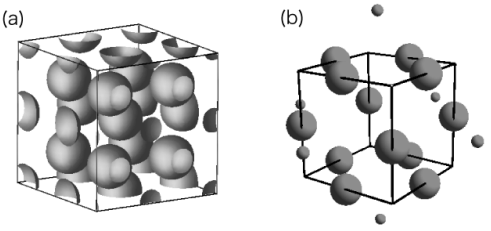

Fig. 5. (a) BCC structure for $\beta = 0.085$ and $L = 2.022 \times 10^{-1}$ ($\delta x = 6.32 \times 10^{-3}$) represented by the isosurface of $u = 0.05$ and (b) the Bragg position with intensities. The details of (b) are the same as those in Fig. 2 (e).

Fig. 3 (b) were identified as Fddd structures. Thus we conclude that this structure is an Fddd structure.

The stationary structure of P is displayed in Fig. 4 together with the Bragg peak positions. The intensities of the higher-order peaks decreased more slowly than those of the Fddd structure. This layer structure has holes in each layer and is identified as a so-called perforated lamellar structure.

We have examined the positions of holes in each layer of this structure. It is evident from this figure that the holes are located at the same position every two layers.

The spherical domains are distinguished by the arrangement of the spheres. The stationary structure of B is displayed in Fig. 5 together with the Bragg position. In Fig. 5 the spheres are located in the center of the body in the fundamental unit. Thus this is a BCC structure.

The stationary structure of Fc is displayed in Fig. 6 together with the Bragg positions. In Fig. 6, the spheres are located at the center of the face in the fundamental unit. Thus this is an FCC structure.

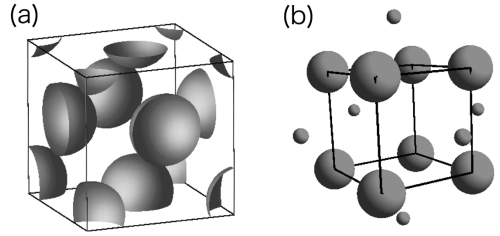

Fig. 6. (a) FCC structure for $\beta = 0.085$ and $L = 1.146 \times 10^{-1}$ ($\delta x = 3.58 \times 10^{-3}$) represented by the isosurface of $u = 0.05$ and (b) the Bragg position with intensities. The details of (b) are the same as those in Fig. 2 (e).

4. Stability analysis of asymptotic solutions

As mentioned above, several structures can coexist for a fixed set of parameters. Hereafter, we explore one of the basic questions to arise in the determination of the most stable structures.

Equations (1) and (2) are the nonequilibrium system. The general method for stability analysis of patterns obtained by nonequilibrium systems is to observe the motion of the planar interface separating between two different structures. If one of the structures invades the other, one may conclude that the former is more stable than the latter. However, to carry out this simulation, one needs to provide a sufficient large system for numerical simulations. This is beyond our computer facilities.

Here, we employ another method to evaluate the stability of obtained structures, in which we derive an approximate Lyapunov functional for equations (1) and (2) used in [11, 12].

4.1. Stability analysis using a mode expansion method

In the limit $\gamma, D_v \to \infty$ with γ/D_v finite, one may formally put $\partial v/\partial t = 0$ in (1), so that the variable v can be eliminated. We thus obtain

$$\frac{\partial u}{\partial t} = -\frac{\delta F}{\delta u}, \tag{7}$$

where

$$\begin{aligned} F\{u\} = \int d\vec{r}\left[\frac{D_u}{2}\left(\vec{\nabla}u\right)^2 - \frac{u^2}{2} + \frac{u^4}{4}\right] \\ + \frac{\gamma}{2D_v}\int d\vec{r}\int d\vec{r}\,' G(\vec{r},\vec{r}\,')(u(\vec{r},t)-\beta)(u(\vec{r}\,',t)-\beta). \end{aligned} \tag{8}$$

The Green function is defined through

$$\left(-\nabla^2 + \frac{\alpha\gamma}{D_v}\right)G(\vec{r},\vec{r}\,') = \delta(\vec{r}-\vec{r}\,'). \tag{9}$$

Since γ/D_v is positive, the functional F plays the role of a Lyapunov functional for the reduced equation (7). This method was first introduced by Ohta [22].

Although the Lyapunov functional (8) is an approximation for the original reaction-diffusion equations of (1) and (2) in the limit of $\gamma, D_v \to \infty$, we attempt to investigate the relative stability of Turing structures by this form.

Here we also approximate the asymptotic solutions by using mode expansion for the variable u which was used in [21]. By expanding of equation (6), a gyroid solution can be approximately expressed a

$$u(\vec{r},t) = u_0 + \left[\sum_{m=1}^{12} a_m(t) e^{i\vec{q}_m \cdot \vec{r}} + \sum_{n=1}^{6} b_n(t) e^{i\vec{p}_n, \vec{r}} + c.c \right], \tag{10}$$

where $a_m(t)$ and $b_n(t)$ is real amplitude. *c.c.* refers to a complex conjugate. The fundamental reciprocal lattice vectors as

$$\begin{aligned}
&\vec{q}_1 = C_Q(2,-1,1), \quad \vec{q}_2 = C_Q(-2,1,1), \quad \vec{q}_3 = C_Q(-2,-1,1),\\
&\vec{q}_4 = C_Q(2,1,1), \quad \vec{q}_5 = C_Q(-1,-2,1), \quad \vec{q}_6 = C_Q(1,-2,1),\\
&\vec{q}_7 = C_Q(-1,2,1), \quad \vec{q}_8 = C_Q(1,2,1), \quad \vec{q}_9 = C_Q(1,-1,-2),\\
&\vec{q}_{10} = C_Q(1,1,-2), \quad \vec{q}_{11} = C_Q(-1,1,-2), \quad \vec{q}_{12} = C_Q(-1,-1,-2),\\
&\vec{p}_1 = C_p(2,2,0), \quad \vec{p}_2 = C_p(2,-2,0), \quad \vec{p}_3 = C_p(0,2,2),\\
&\vec{p}_4 = C_p(0,-2,2), \quad \vec{p}_5 = C_p(2,0,2), \quad \vec{p}_6 = C_p(-2,0,2),
\end{aligned}$$

where the coefficients are chosen as $C_Q = Q/\sqrt{6}$, $C_P = P/(2\sqrt{2})$ so that $|\vec{q}_i| = Q$, $|\vec{p}_i| = P$ and $Q^2 = 3P^2/4$.

Lamellar, hexagonal, BCC, and Fddd structures obtained by using parameters near Turing bifurcation can be represented as substructures composed of combinations whose reciprocal vectors are contained in the 18 modes of a gyroid.

Note that the approximation of asymptotic solution of Fddd is less accuracy because the intensity of higher harmonics is not necessarily negligible, and the asymptotic solution of perforated lamellar cannot be expressed by the 18 modes of equation (10) since the intensity of the modes gradually changes.

Nevertheless, substituting equation (8) into (10) and ignoring the higher harmonics, we obtain the Lyapunov functional in terms of the amplitudes and magnitudes of the reciprocal vectors, $F_{\mathrm{mode}} = F(\{a_m\}, \{b_n\}, P)$. This explicit form is too lengthy to be written here. Through the minimization of F_{mode} with respect to a_m, b_n and P, we may determine the most stable structure for fixed parameters in the reduced system (7). The result is summarized in Fig. 7.

4.2. Stability analysis of the direct simulation of the time evolution equation

In the previous section we evaluated the stability of the asymptotic domains by using the mode-expansion method. However, one cannot use this method to evaluate the stability of perforated lamellar. In this section, therefore, we carry out direct numerical simulation of the Lyapunov functional equation (8).

It should be noted that the most stable period of structures is unknown before the equation is solved. Therefore, we have to repeat simulations by changing the

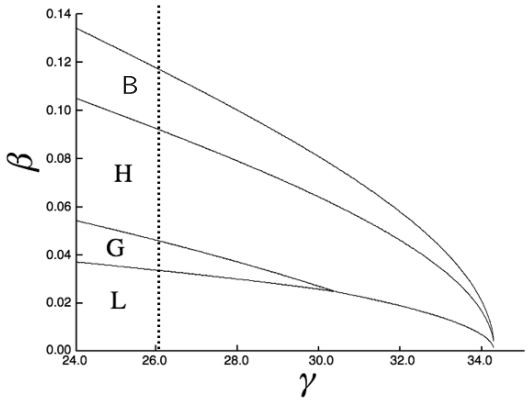

Fig. 7. Phase diagram in the $\gamma-\beta$ plane. The most stable regions for lamellar, hexagonal, gyroid and BCC are indicated by L, H, G, and S, respectively.

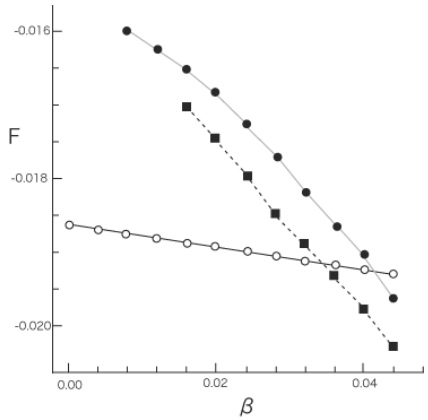

Fig. 8. The lowest values of the Lyapunov functional introducing lamellar (white circle). Gyroid (square) and perforated lamellar (black circle) structures for $\gamma = 26.0$. The lines for the gyroid and perforated lamellar are terminated at some value β, beyond which these stable solutions do not exist.

domain size to find the optimal size, i.e., that which gives us the lowest values for the Lyapunov functional equation (8) to introduce each structure. We evaluate the three solutions of lamellar, gyroid, and perforated lamellar as patterns to investigate the most stable structure in the range where the perforated lamellar domain is obtained. Substituting these solutions into the Lyapunov functional equation (8), the lowest value of each structure can be calculated. Fig. 8 displays the results for $D_u = 5.0\times10^{-5}$, $D_v = 5.0\times10^{-3}$, $\alpha = 0.5$, and $\gamma = 26$. The horizontal and vertical axes are the control parameter β and the value of the Lyapunov functional per unit volume, respectively. It is evident from this figure that there is no range where the value of the Lyapunov functional per unit volume of the perforated lamellar is the

lowest. Therefore, we may judge that perforated lamellar is not the most stable structure in the case where $D_u = 5.0 \times 10^{-5}$, $D_v = 5.0 \times 10^{-3}$, $\alpha = 0.5$, and $\gamma = 26$.

5. Discussion

We have studied Turing patterns arising in the FitzHugh–Nagumo type reaction-diffusion equation in three dimensions. Apart from lamellar and hexagonal structures, which are simple generalizations of two-dimensional patterns, we have obtained gyroid, Fddd, BCC, FCC, and perforated lamellar structures. Except for the BCC and FCC structures, the domains consist of interconnected networks that are characteristic of three dimensions.

It is emphasized that the domain size is to be one of the important factors in three-dimensional patterns, because there are more varieties of structures in three-dimensions than that in two dimensions and the fundamental periods of structures are a little bit different among them. To prevent the dependency on domain size, we need to provide a sufficient large system for numerical simulation. That is beyond our computer facilities. That is why we here focus on the fundamental periodic patterns of each structure.

This paper has also addressed the stability analysis of the obtained domains. We employ a method to derive approximately the Lyapunov functional equation (8) for equations (1) and (2) following the manner in [23]. Evaluating the Lyapunov functional of each structure using the mode-expansion method the theoretical phase diagram shown in Fig. 7. Moreover, by using the direct simulations of Lyapunov functional introducing obtained distributions, we conformed there are no parameter range in $D_u = 5.0 \times 10^{-5}$, $D_v = 5.0 \times 10^{-3}$, $\alpha = 0.5$, and $\gamma = 26$ where a perforated lamellar would be the most stable structure.

Acknowledgments. This work was supported in part by a Grant-in-Aid from the Japan Society for the Promotion of Science to H.S. and one to K.Y. The numerical calculations were carried out on Altix 3700 BX2 at YITP, Kyoto University. We also thank the following people for their helpful comments: Prof. T. Ohta, and Dr. D. Ueyama.

References

[1] H. Meinhardt, Models of Biological Pattern Formation. Academic Press, London, 1982.
[2] J.D. Murray, Mathematical Biology. Springer-Verlag, New York, 2003.
[3] A.M. Turing, The chemical basis of morphogenesis. Phil. Trans. R. Soc. Lond. B, **237** (1952), 37–72.
[4] G. Nicolis and I. Prigogine, Self-Organization in Nonequilibrium Systems. Wiley, New York, 1977.
[5] P. De Kepper, E. Dulos, J. Boissonade, A. De Wit, G. Dewel and P. Borckmans, Reaction-diffusion patterns in confined chemical systems. J. Stat. Physic., **101** (2000), 495–508.
[6] V. Castets, E. Dulos, J. Boissonade and P. De Kepper, Experimental-evidence of a sustained standing Turing-type nonequilibrium chemical-pattern. Phys. Rev. Lett., **64** (1990), 2953–2956.
[7] H. Haken, Synergetics, An Introduction. Springer-Verlag, Berlin, 1977.

[8] A. De Wit, G. Dewel, P. Borckmans and D. Walgraef, 3-dimensional dissipative structures in reaction diffusion-systems. Physica D., **61** (1992), 289–296.
[9] A. De Wit, P. Borckmans and G. Dewel, Twist grain boundaries in three-dimensional lamellar Turing structures. Proc. Nat. Acad. Sci., **94** (1997), 12765–12768.
[10] T. Leppanen, M. Karttunen, R. Kaski, R. A. Barrio and L. Zhang, A new dimension to Turing patterns. Physica D., **168** (2002), 35–44.
[11] H. Shoji, K. Yamada and T. Ohta, Interconnected Turing patterns in three-dimensions. Phys. Rev. E, **72** (2005), 65202(R).
[12] H. Shoji, K. Yamada, D. Ueyama and T. Ohta, in review.
[13] R. FitzHugh, Impulses and physiological states in theoretical models of nerve membrane. Biophys. J., **9** (1961), 445–466.
[14] J. Nagumo, R. Arimoto and S. Yoshizawa, Active pulse transmission line simulating nerve axon. Proc. IRE, **50** (1962), 2061–?.
[15] J. Rinzel and J.B. Keller, Travelling-wave solutions of a nerve-conduction equation. Biophys., **13** (1973), 1313–1337.
[16] J.J. Tyson and J.P. Keener, Singular perturbation-theory of traveling waves in excitable media. Physica D., **32** (1988), 327–361.
[17] I. Prigogine and R. Lefever, Symmetry breaking instabilities in dissipative systems. 2. J. Chem. Phys., **48** (1968), 1695–1700.
[18] P. Gray and S.K. Scott, Autocatalytic reactions in the isothermal, continuous stirred tank reactor-isolas and other forms of multistability. Chem. Eng. Sci., **38** (1983), 29–43.
[19] A. Shinozaki and Y. Oono, Spinodal decomposition in 3-space. Phys. Rev. E, **48** (1993), 2622–2654.
[20] A. Aksimetiev, M. Fialkovski and R. Holyst, Morphology of surfaces in mesoscopic polymers, surfactants, electrons, or reaction-diffusion systems: Methods, simulations, and measurements. Adv. Chem. Phys., **121** (2002), 141–239.
[21] K. Yamada, M. Nonomura and T. Ohta, Kinetics of morphological transitions in microphase-separated diblock copolymers. Macromolecules, **37** (2004), 5762–5777.
[22] T. Ohta, Decay of metastable rest state in excitable reaction-diffusion system. Prog. Theo. Phys. Suppl., **99** (1989), 425–441.